
Weights to Code: Extracting Interpretable Algorithms from the Discrete Transformer

Yifan Zhang^{1,2†} Wei Bi³ Kechi Zhang^{1,2} Dongming Jin^{1,2} Jie Fu^{4,5} Zhi Jin^{1,2}

Abstract

Algorithm extraction aims to synthesize executable programs directly from models trained on algorithmic tasks, enabling *de novo* algorithm discovery without relying on human-written code. However, applying this paradigm to Transformer is hindered by representation entanglement (e.g., superposition), where entangled features encoded in overlapping directions obstruct the recovery of symbolic expressions. We propose the Discrete Transformer, an architecture explicitly designed to bridge the gap between continuous representations and discrete symbolic logic. By injecting discreteness through temperature-annealed sampling, our framework effectively leverages hypothesis testing and symbolic regression to extract human-readable programs. Empirically, the Discrete Transformer achieves performance comparable to RNN-based methods while extending interpretability to continuous variable domains, and the annealing dynamics exhibit a clear exploration-to-exploitation transition. Finally, we show that architectural inductive biases provide fine-grained control over synthesized programs, establishing the Discrete Transformer as a robust framework for demonstration-free algorithm discovery and Transformer interpretability.

1. Introduction

Program synthesis is the task to construct a program that provably satisfies a given high-level formal specification, a long-standing problem which can date back to Church (1963). In recent years, this field has been revolutionized by Large Language Models (LLMs), which have achieved

[†]Work done during an internship at Kuaishou Technology. ¹Key Laboratory of High Confidence Software Technology (PKU), MOE, Beijing, China ²School of Computer Science, Peking University, Beijing, China ³Kuaishou Technology, Beijing, China ⁴Shanghai AI Lab, Shanghai, China ⁵Shanghai Innovation Institute, Shanghai, China. Correspondence to: Jie Fu <fu-jie@pjlab.org.cn>, Zhi Jin <zhijin@pku.edu.cn>.

remarkable success in code generation (Rozière et al., 2024; Guo et al., 2024; CodeGemma Team et al., 2024). Despite their success, an alternative paradigm—*algorithm extraction*—offers a distinct advantage: the ability to derive algorithms *de novo*, thereby potentially uncovering innovative solutions that are independent of human-generated data (Michaud et al., 2024). Recent work has demonstrated the feasibility of this approach in Recurrent Neural Networks (RNNs) via the Mechanistic-Interpretability-based Program Synthesis (MIPS), which successfully leverages symbolic regression to synthesize programs that accurately match neural network behavior (Michaud et al., 2024).

However, extending algorithm extraction to the dominant Transformer architecture faces significant challenges, rooted in a fundamental gap between the continuous, high-dimensional nature of Transformer and the discrete, sparse nature of symbolic algorithms. The primary obstacle lies in interpreting the Transformer’s internal representations. Specifically, the standard Transformer often exhibits “superposition”, where features are encoded in an overlapping, non-orthogonal set of directions rather than individual neurons (Cunningham et al., 2023; Elhage et al., 2022). Consequently, the model’s internal representations are highly entangled and polysemantic. Unlike the disentangled input-output mappings required for symbolic regression, these representations render the direct extraction of explicit symbolic expressions infeasible. This motivates our central question: *Is it possible to synthesize executable and interpretable programs by extracting algorithms from Transformer?*

In this work, we propose the *Discrete Transformer*, an architecture explicitly optimized for algorithm extraction (see Figure 1). Building upon the framework of Transformer Programs (Friedman et al., 2023), our design incorporates critical modifications to facilitate the transition from continuous dynamics to discrete logic. Architecturally, the Discrete Transformer comprises the Numerical Attention, Numerical MLP, and linear output head. Aligning with the Restricted Access Sequence Processing (RASP) computational model (Weiss et al., 2021), we impose a strict functional disentanglement, where the Numerical Attention is responsible for routing information across positions, while the Numerical MLP is dedicated solely to element-wise arithmetic operations. Crucially, we incorporate differ-

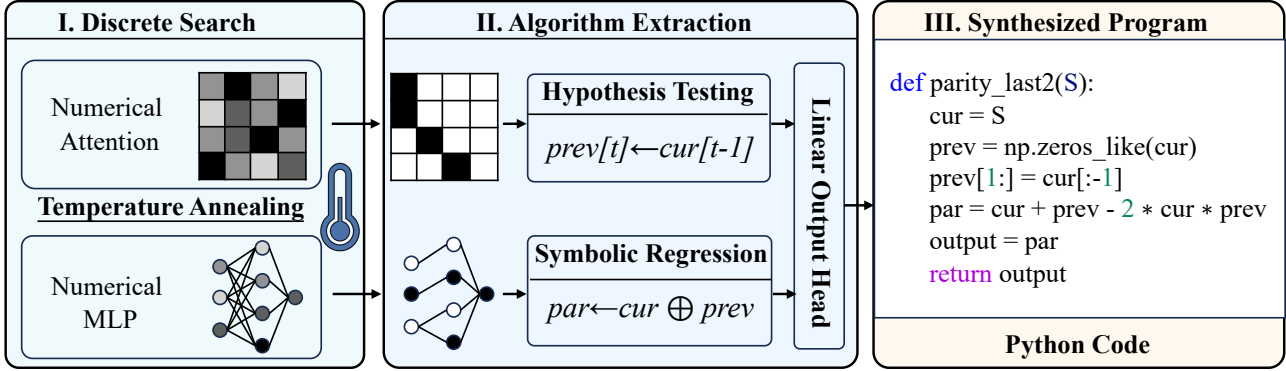


Figure 1. Illustration of the proposed framework for extracting executable algorithms from a Discrete Transformer. (I) Discrete Search: Temperature annealing is leveraged to encourage interpretable discretization in both Numerical Attention and MLP modules. (II) Algorithm Extraction: Attention patterns are characterized via hypothesis testing, while arithmetic transformations are approximated through symbolic regression. (III) Synthesized Program: The extracted components are integrated via a linear output head to generate Python code. As shown, the framework successfully recovers the `parity_last2` algorithm, correctly implementing the arithmetic XOR logic.

entiable sampling mechanisms into each module to inject temperature-controlled discreteness. Through annealing, the model gradually transitions into a fully discrete computation graph, ensuring that the solution to the algorithmic task is implicitly but clearly encoded within its weights.

Once the model converges to a discrete state, we employ a modular strategy to recover the underlying algorithm. Recognizing the distinct roles of the components, we adopt *hypothesis testing* for the Numerical Attention modules to identify interpretable routing patterns, and apply *symbolic regression* to the Numerical MLP modules to infer the specific arithmetic expressions. Finally, these extracted primitives are aggregated through the linear output head, yielding a concise, human-readable, and executable program that verifiably solves the target task.

We validate our approach across a diverse suite of algorithmic tasks, achieving comparable algorithm extraction performance to the RNN-based prior method (MIPS). Crucially, unlike MIPS, which is constrained by discrete latent-variable approximations, our Discrete Transformer natively processes continuous latent variables, substantially broadening the scope of mechanistic-interpretability-based program synthesis. Beyond performance, we provide a rigorous analysis of the framework’s theoretical and empirical properties. In addition to revealing that functional convergence precedes full structural discretization (Louizos et al., 2018; Savarese et al., 2021), we demonstrate that tailoring architectural constraints imposes strong inductive biases, establishing the Discrete Transformer as a controllable framework for interpretable algorithm discovery.

Overall, our main contributions are as follows:

- We propose the Discrete Transformer, a RASP-aligned

architecture that enforces functional disentanglement to bridge continuous optimization and discrete logic.

- We develop a modular extraction pipeline combining hypothesis testing and symbolic regression, extending mechanistic-interpretability-based synthesis to continuous variables.
- We provide rigorous analysis validating the effectiveness of imposed inductive biases for controllable algorithm discovery.

2. Related Work

2.1. Mechanistic Interpretability in Transformer

The foundation for connecting Transformer with programs is the RASP (Weiss et al., 2021), which abstracts sequence processing into primitives. Building on this abstraction, Tracr (Lindner et al., 2023) compiles such programs *into* Transformer weights, whereas Transformer Programs (Friedman et al., 2023) tackle the inverse problem of *learning* interpretable structures. By imposing strict architectural constraints and employing Gumbel-Softmax optimization (Jang et al., 2017) to encourage discretization, this approach produces models that can be deterministically mapped to programs. Despite the resulting executable programs, their representations are inherently bounded (e.g., finite-grid or categorical logic) and thus do not naturally capture open-form algebraic logic targeted by our symbolic regression-based extraction.

2.2. Symbolic Regression and Algorithm Extraction

Symbolic regression searches for closed-form expressions balancing accuracy and complexity (Udrescu et al., 2020;

Cranmer, 2023). While traditionally used for scientific discovery (Cranmer et al., 2020; Ma et al., 2022) or recently enhanced by LLMs’ scientific priors (Shojaee et al., 2025), we leverage it as the core engine for algorithm extraction—synthesizing concise, readable programs directly from trained neural networks.

The innovative MIPS framework (Michaud et al., 2024) pioneers this approach for RNNs. Analogous to the use of Sparse Autoencoders (SAEs) in interpreting features (Cunningham et al., 2023; Bricken et al., 2023), the MIPS employs post-hoc integer autoencoders to approximate continuous latent states into finite states suitable for symbolic regression. In contrast to the MIPS, which relies on auxiliary quantization modules to approximate discreteness, our Discrete Transformer is architecturally designed to learn an interpretable, inherently discrete computation graph, thereby enabling direct and seamless algorithm extraction.

3. Discrete Transformer

In this section, we introduce the Discrete Transformer, a specialized architecture purposefully designed for symbolic regression and algorithm extraction. It is structured as a computational graph with clear functional specialization: the Numerical Attention performs explicit variable routing, while the Numerical MLP is responsible for arithmetic computation.

3.1. Numerical Residual Stream

The essential difference between the Discrete Transformer and the standard one lies in the structure of the residual stream and the mechanism of information processing. To align with the symbolic nature of algorithm extraction, we define the residual stream not as latent vectors, but as a collection of explicit scalar variables. Let $\mathbf{h}_l = [x_1, \dots, x_{N_l}]^\top \in \mathbb{R}^{N_l}$ denote the residual stream at layer l , consisting of N_l distinct scalar variables. In contrast to standard additive updates, we adapt the concatenation principle (Friedman et al., 2023; Lai-Dang et al., 2025) to the scalar domain, updating the residual stream with new outputs \mathbf{o}_l :

$$\mathbf{h}_{l+1} = \text{Concat}(\mathbf{h}_l, \mathbf{o}_l) \in \mathbb{R}^{N_l + |\mathbf{o}_l|}. \quad (1)$$

This design preserves the full computational history as disentangled coordinates, alleviating the information interference induced by superposition in dense vectors.

Moreover, a critical challenge in algorithm extraction is to identify *which* variables serve as operands. Inspired by learnable input selection (Friedman et al., 2023), we address this by designing a discretized reading mechanism tailored for the numerical residual stream: for any computational module (Numerical Attention or MLP) at layer l requiring

k inputs, we learn a projection matrix $\mathbf{W}_{\text{read}} \in \mathbb{R}^{k \times N_l}$ to select inputs from the residual stream \mathbf{h}_l . To enable discrete structure optimization within a differentiable framework, we apply a temperature-controlled sampling function $S(\cdot, \tau)$ (derivation provided in Appendix A) row-wise to the logits $\mathbf{W}_{\text{read}} \mathbf{h}_l$. The input vector $\mathbf{u} \in \mathbb{R}^k$ is then retrieved from the current residual stream $\mathbf{h}_l \in \mathbb{R}^{N_l}$ via:

$$\mathbf{u} = S(\mathbf{W}_{\text{read}}, \tau) \mathbf{h}_l, \quad (2)$$

where τ is the annealing temperature. As temperature $\tau \rightarrow 0$, the selection distribution converges to a deterministic one-hot indicator, effectively functioning as a differentiable pointer over the computation graph.

3.2. Numerical Attention as Router

Following the architectural paradigm established in Tracr (Lindner et al., 2023) and Transformer Programs (Friedman et al., 2023), we employ a hard attention mechanism designed strictly as an information routing operator, rather than a feature mixer. In the context of algorithm extraction, this design can help isolate all computational transformations within the Numerical MLP, thereby reducing the difficulty of attention analysis.

Piecewise Linear Encoding. Since the residual stream consists of raw scalars ($\mathbf{h}_l \in \mathbb{R}^{N_l}$), distinct scalar variables lack the high-dimensional expressivity required for effective dot-product comparisons. To address this, we define the query and key as selected scalars $x_q, x_k \in \mathbb{R}$, and project them into a higher-dimensional space using the Piecewise Linear Encoding (PLE) (Gorishniy et al., 2022):

$$\mathbf{q} = \phi_{\text{PLE}}(x_q), \quad \mathbf{k} = \phi_{\text{PLE}}(x_k), \quad (3)$$

where $\mathbf{q}, \mathbf{k} \in \mathbb{R}^{d_{\text{attn}}}$ and $\phi_{\text{PLE}} : \mathbb{R} \rightarrow \mathbb{R}^{d_{\text{attn}}}$ is a learnable mapping.

Deterministic Attention Mechanism. The attention scores $\mathbf{a}_{\text{raw}} \in \mathbb{R}^T$ over a context length T are computed via scaled dot-product with T5-style relative positional biases \mathbf{b}_{rel} (Rafael et al., 2023):

$$\mathbf{a}_{\text{raw}} = \frac{\mathbf{K}\mathbf{q}}{\sqrt{d_{\text{attn}}}} + \mathbf{b}_{\text{rel}}, \quad (4)$$

where $\mathbf{K} \in \mathbb{R}^{T \times d_{\text{attn}}}$ stacks the projected keys from the context. To ensure interpretable attention patterns, we enforce hard attention using the sampling function $S(\cdot, \tau)$. Crucially, the value projection is the identity function for scalars, meaning that the value vector $\mathbf{v} \in \mathbb{R}^T$ consists directly of the raw scalars from the history. The output $o_{\text{attn}} \in \mathbb{R}$ is a weighted sum:

$$o_{\text{attn}} = S(\mathbf{a}_{\text{raw}}, \tau)^\top \mathbf{v}. \quad (5)$$

This design forces the attention head to converge to a deterministic pointer operation, retrieving specific raw values

from history (e.g., “copy the value from the token at offset -1”).

3.3. Numerical MLP as Operator

While the Numerical Attention handles data movement, the Numerical MLP is dedicated to element-wise arithmetic and logical transformations. Drawing on the insight that Transformer MLPs contribute additive updates to the residual stream, which can be decomposed into weighted sums of sub-updates (Geva et al., 2022), we explicitly decompose the MLP module into a collection of parallel, independent sub-modules (sub-MLPs).

Each sub-module performs a single elementary operation. It first selects a small, fixed number of scalars (typically $k = 2$) from the stream via the discretized reading mechanism, forming an operand vector $\mathbf{u} \in \mathbb{R}^k$. These operands are processed by a shallow network:

$$o_{\text{mlp}} = \mathbf{W}_2 \sigma(\mathbf{W}_1 \mathbf{u} + \mathbf{b}_1) + b_2, \quad (6)$$

where $\mathbf{W}_1 \in \mathbb{R}^{d_{\text{hid}} \times k}$, $\mathbf{W}_2 \in \mathbb{R}^{1 \times d_{\text{hid}}}$ are learnable weights, \mathbf{b}_1, b_2 are biases, and σ is a non-linear activation (e.g., ReLU). The resulting scalar output o_{mlp} is concatenated back to the residual stream.

Inductive Bias for Symbolic Regression. By severely constraining the input dimension k and the hidden width d_{hid} , we deliberately limit the complexity of each sub-module. This bottleneck forces the network to decompose complex functions into a sequence of simple arithmetic steps, creating ideal conditions for symbolic regression (e.g., PySR (Cranmer, 2023)) to extract closed-form expressions.

3.4. Linear Output Head

The architecture concludes with a linear output head that aggregates the discrete computational steps into a final prediction:

$$\hat{y} = \mathbf{w}_{\text{out}}^T \mathbf{h}_{\text{final}}, \quad (7)$$

where $\mathbf{h}_{\text{final}}$ is the final residual stream, and \mathbf{w}_{out} represents the aggregation weights. The final trained model thus represents a clean, executable computational graph: nodes correspond to either routing operations (Numerical Attention) or arithmetic functions (Numerical MLP), and edges are defined by the discrete selections of the discretized reading modules.

4. From Weights to Code

After training with temperature annealing, the converged Discrete Transformer reaches a fully discrete state, and the algorithmic solution is implicitly encoded within its sparse weights and activation patterns. To recover an explicit, human-readable program, we treat the trained model

as a computational graph composed of two distinct types of nodes: *routers* (Attention) and *operators* (MLP). We propose a decoupled extraction pipeline that first infers the function of each node using component-specific strategies, then reconstructs the global program trace via backward traversal.

4.1. Hypothesis Testing for Numerical Attention

For the Numerical Attention module, directly extracting explicit symbolic expressions via symbolic regression is challenging due to the computational complexity introduced by the PLE of queries and keys, dot-product interactions, and the hard attention mechanism induced by sampling functions. However, since the structural role of attention is constrained to be an information router, we abstract away from the intermediate arithmetic operations and focus our interpretability analysis on the resulting routing patterns.

We conceptualize the Numerical Attention module as a deterministic pointer performing differentiable addressing on context memory. Following Neural Turing Machines (Graves et al., 2014), we categorize addressing into *Location-based* and *Content-based*. We hypothesize that our attention heads specialize into these two modes, and empirically observe that they manifest as two typical interpretable patterns: *Fixed Offset* and *Windowed Extrema*.

Specifically, for a given head, we analyze its attention matrices generated over the validation set and test the hypotheses by examining the statistical properties:

- *Fixed Offset.* This pattern corresponds to relative positional indexing. We hypothesize that there exists an integer offset δ such that, for a large fraction of query positions i , the head places most of its attention on $j = i - \delta$. We operationalize this by measuring whether the averaged attention mass concentrates on a single offset diagonal (corresponding to $j = i - \delta$) beyond a predefined threshold.
- *Windowed Extrema.* This pattern reflects content-dependent selection. Let $\mathbf{v} \in \mathbb{R}^T$ be the sequence of scalar values, where v_j is the value at position j . We hypothesize that there exists a window size $z \in \mathbb{Z}^+$ such that, for a large fraction of query positions i , the head primarily attends to $j^* = \arg \min / \max_{j \in \{i-z+1, \dots, i\}} v_j$. We verify this hypothesis by checking the sample-wise agreement between the head’s selected index and the true extremum index within the window.

There might exist “unmatched heads”; however, across the algorithm benchmark, we find that they represent computational noise—being negligible in magnitude or acting as redundant variables—and do not influence the logic of the

final assembled program (see Appendix B for detailed analysis).

4.2. Symbolic Regression for Numerical MLP

In contrast to the Numerical Attention, the Numerical MLP modules serve as the arithmetic core. Thanks to the disentangled architecture, each MLP sub-module functions as an isolated mapping $f : \mathbb{R}^k \rightarrow \mathbb{R}$ with low-dimensional inputs (typically $k = 2$). This architectural isolation makes them ideal candidates for black-box symbolic regression.

For each sub-MLP, we collect a dataset of input-output pairs $\mathcal{D} = \{(\mathbf{u}^{(i)}, o_{\text{mlp}}^{(i)})\}_{i=1}^M$ from validation passes. We employ the PySR (Cranmer, 2023), a symbolic regression tool based on genetic algorithms, to search for the optimal symbolic expression \hat{f} that minimizes the error on \mathcal{D} . Crucially, the constrained input dimension and limited model capacity drastically reduce the search space, enabling the PySR to reliably converge to exact arithmetic expressions (e.g., $o_{\text{mlp}} = 2u_1 + u_2$) rather than approximate fits.

4.3. Global Program Assembly

The final phase integrates these extracted primitives into a coherent program. The linear output head, $\hat{y} = \mathbf{w}_{\text{out}}^\top \mathbf{h}_{\text{final}}$, serves as the entry point for extraction. To reduce the length of the extracted program, we impose a sparsity threshold ϵ on the magnitude of the weights \mathbf{w}_{out} . This prunes unnecessary variables from the computation graph, retaining the active variables contributing to the final prediction.

Starting from these active variables, we perform a *backward traversal* of the computational graph. Recursively, we replace each intermediate variable in the residual stream with its corresponding symbolic definition, either a deterministic pointer from the Numerical Attention or a distilled arithmetic expression from the Numerical MLP, until the traversal reaches the raw input tokens. This process effectively compiles the neural network into concise, closed-form algorithmic expressions that approximate the Discrete Transformer’s behavior with high fidelity across the relevant input domain.

5. Experiments

In this section, we evaluate the Discrete Transformer on a diverse suite of algorithmic reasoning tasks. We aim to demonstrate that, beyond achieving high predictive performance, our model extracts interpretable and human-readable algorithms with high fidelity, thereby revealing the underlying structure and logic inherent in the data.

Datasets We construct an algorithmic reasoning benchmark designed to evaluate symbolic rule recovery across a range of capabilities, including arithmetic reasoning, variable

tracking, and non-linear composition. The tasks are primarily sourced from the MIPS benchmark (Michaud et al., 2024), excluding those whose ground-truth rules cannot be expressed using general symbolic operators (e.g., the palindrome rule in `bit_palindrome`).¹ To broaden coverage of continuous-valued physical dynamics, we additionally introduce two tasks, `exponential_moving_average` and `free_fall_height`. We group all tasks into three categories based on their underlying logic: (1) *Linear Arithmetic* (e.g., `sum_last2`, `gravity`), which involves learning linear mathematical or physical logic; (2) *Non-Linear Composition* (e.g., `parity_last2`, `add_mod_3`), which requires approximating non-linear logic; and (3) *Continuous Dynamics* (e.g., `exponential_moving_average`), which assess the capability to model tasks with floating-point variables. Detailed task definitions are provided in Appendix Table 2.

Training Details All models adopt a decoder-only architecture implemented in PyTorch, optimized via AdamW to minimize the mean squared error (MSE). We train for 50 epochs with a batch size of 512 and cosine learning rate decay. Crucially, to handle discrete optimization, we apply geometric annealing to the sampling temperature τ , decreasing it from 10.0 to 0.1. We report the average performance across three random seeds, with hyperparameters (layers, heads, sub-MLPs) selected via grid search. Full experimental details are provided in Appendix C.

Results The Discrete Transformer demonstrates strong predictive performance across most of the algorithmic tasks, with MSE approaching zero (see Appendix Table 2). Beyond prediction, our primary contribution is to show that the solutions encoded in the Discrete Transformer can be *explicitly* extracted into human-readable code. Specifically, by applying the methodology described in Section 4, we successfully distill executable Python programs from the trained weights. As shown in Table 1, the extracted programs successfully solve most algorithmic tasks, achieving an accuracy of 1.00, which matches the performance of MIPS. Moreover, the low root mean squared error (RMSE) further indicates the high fidelity of our extraction methodology. Notably, the Discrete Transformer additionally handles continuous-dynamics tasks that lie beyond the scope of MIPS. We summarize three key findings below.

- **Discovery of Algorithmic Mechanisms in Linear Tasks.** For linear tasks, the discrete optimization process exhibits an efficient ability to discover underlying algorithmic mechanisms. On simple instances, the model frequently learns to bypass the Numeri-

¹Since our goal is to extract closed-form expressions of fixed-size through symbolic regression (typically PySR), we restrict our benchmark to tasks whose ground-truth mappings are representable under PySR’s default operator set (e.g., $+$, $-$, \times , \div).

Table 1. Comparison of algorithm extraction performance between MIPS and the Discrete Transformer (Ours) on the algorithmic benchmark. For integer-valued tasks, we evaluate test-set accuracy (Acc.) by rounding outputs to the nearest integer and report Root Mean Squared Error (RMSE) to assess extraction fidelity. For tasks involving floating-point data types, Acc. is not applicable (N/A) and only RMSE is reported. MIPS results are retrieved from Michaud et al. (2024); † denotes that MIPS fails to achieve perfect accuracy (1.00) or is inapplicable due to inherent limitations.

Task	MIPS		Ours		Task	MIPS		Ours	
	Acc.	Acc.	Acc.	RMSE		Acc.	Acc.	Acc.	RMSE
<i>Linear Arithmetic</i>									
sum_last2	1.00	1.00	1.00	8.22×10^{-5}	diff_last2	1.00	1.00	1.00	2.65×10^{-8}
sum	1.00	1.00	1.00	1.30×10^{-7}	div_3	†	0.67	1.00	4.69×10^{-1}
freebody	1.00	1.00	1.00	9.78×10^{-6}	gravity	1.00	1.00	1.00	4.31×10^{-6}
spring	1.00	1.00	1.00	5.91×10^{-5}	magnetic	†	0.02	1.00	1.06×10^1
<i>Non-Linear Composition</i>									
parity_last2	1.00	1.00	1.00	1.21×10^{-6}	maximum_prev2	1.00	1.00	1.00	2.10×10^{-3}
minimum_prev2	1.00	1.00	1.00	4.21×10^{-3}	unique_prev2	1.00	1.00	1.00	2.05×10^{-7}
bitwise_and	1.00	1.00	1.00	1.03×10^{-9}	bitwise_or	1.00	1.00	1.00	1.28×10^{-3}
bitwise_not	1.00	1.00	1.00	3.80×10^{-9}	bitwise_xor	1.00	1.00	1.00	2.58×10^{-9}
balanced_parenthesis	†	0.98	1.00	1.45×10^{-1}	abs	1.00	1.00	1.00	2.29×10^{-7}
abs_of_diff	1.00	1.00	1.00	1.42×10^{-4}	parity	1.00	1.00	1.00	8.99×10^{-9}
parity_zeros	1.00	1.00	1.00	1.99×10^{-5}	add_mod_3	1.00	1.00	1.00	4.15×10^{-4}
bit_dot_prod_mod_2	1.00	1.00	1.00	1.97×10^{-3}	bit_addition	1.00	0.99	1.00	1.49×10^{-1}
<i>Continuous Dynamics</i>									
exponential_moving_average	†	N/A	1.00	4.04×10^{-7}	free_fall_height	†	N/A	1.00	9.02×10^{-3}

cal MLP entirely, instead leveraging the linear output head to perform arithmetic directly. For instance, in `sum_last2` (Figure 2),² the model assigns specific attention heads to retrieve x_{t-1} (via a verified “Fixed Offset” pattern) and integrates it with the current token x_t . Symbolic simplification yields the exact expression $y_t = x_t + x_{t-1}$,³ effectively capturing the underlying addition logic. On more complex physical tasks such as `gravity`, the model identifies the essential computational variables and constructs the correct computation graph through the coordination of the Numerical Attention, Numerical MLP, and linear output head, demonstrating strong potential for efficient modeling of physical processes.

- **Exact Recovery of Non-Linear Identities.** For tasks requiring non-linear logic, the extraction methodology successfully identifies algebraically equivalent expressions rather than merely producing approximate fits. For instance, in the `parity_last2` task ($x_t \oplus x_{t-1}$) with binary inputs $x \in \{0, 1\}$, simplifying the extracted expressions (Figure 3) yields $y_t = x_t + x_{t-1} - 2x_t x_{t-1}$, which is an exact algebraic formulation of the parity operation. For `maximum_prev2` and `minimum_prev2` tasks, simplifying the extracted

²For clarity of presentation, we round the coefficients of symbolic expressions to two decimal places.

³We employ the SymPy library (Meurer et al., 2017) to automatically simplify the extracted expressions, leading to more concise and readable mathematical formulae.

expressions in Figure 4 reveals a piecewise-linear implementation of conditional computation via ReLU operations: $\max(x_t, x_{t-1}) = x_{t-1} + \text{ReLU}(x_t - x_{t-1})$ and $\min(x_t, x_{t-1}) = x_{t-1} - \text{ReLU}(x_{t-1} - x_t)$. This demonstrates the capability to reverse-engineer black-box neural computations into explicit algebraic forms equivalent to logical operations.

- **Modeling Continuous Dynamics.** Owing to its inherent model design, our framework offers a clear advantage over prior symbolic synthesis approaches. MIPS, in particular, relies on discrete latent-state abstractions and is therefore not directly applicable to floating-point data types. In contrast, the Discrete Transformer natively operates on continuous variables, allowing the extracted programs to preserve real-valued intermediate computations rather than forcing discretization. This distinction enables the extraction of algorithms that capture continuous dynamics in tasks such as `exponential_moving_average` and `free_fall_height`, substantially broadening the scope of mechanistic-interpretability-based program synthesis.

To evaluate the robustness of our framework under architectural variations, we examine how key hyperparameters (e.g., the number of heads) influence both convergence (MSE) and program complexity (measured by the line count). Our results indicate that, once the architecture meets the minimal functional requirements of the task, the Discrete Trans-

```

1 import numpy as np
2 def sum_last2(input_seq):
3     # V0_input
4     input_arr = np.array(input_seq, dtype
5                           =float)
6     seq_len = input_arr.shape[0]
7     V0 = input_arr[:, 0]
8     # V1_Attn_LOH0
9     V1 = np.zeros(seq_len)
10    # Fixed offset 1
11    V1[1:] = V0[:-1]
12    # V2_Attn_LOH1
13    V2 = np.zeros(seq_len)
14    # Fixed offset 1
15    V2[1:] = V0[:-1]
16    # Output Head
17    output = 1.00 * V0 + 1.00 * V1 + 0.01
18           * V2
19    return output
    
```

↓ *symbolic simplification*

Simplified Expression: $y_t = x_t + x_{t-1}$

Figure 2. Algorithm extraction results for the `sum_last2` task. Modules are denoted by their type and indices (e.g., `Attn_LOH0` represents the attention head at index 0 of layer 0). The extracted code reveals that the model utilizes specific attention heads to retrieve the previous token. Symbolic simplification (bottom) shows the mathematically simplified expression, verifying that the model correctly learns the logic $y_t = x_t + x_{t-1}$.

former consistently converges to a near-zero MSE loss and yields executable extracted programs, demonstrating strong robustness. Additional details are provided in Appendix D.

6. Further Analysis

In this section, we provide a rigorous analysis of the Discrete Transformer’s properties, positioning it at the intersection of program synthesis and continuous sparsification. We primarily focus on the training dynamics, characterizing a distinct phase where functional convergence is achieved prior to complete structural discretization. We further demonstrate how architectural constraints serve as strong inductive biases, establishing the model as a controllable testbed for interpretable algorithm discovery.

6.1. Continuous-to-Discrete Homotopy

We frame program synthesis as a continuous-to-discrete homotopic transformation. From the perspective of differentiable architecture search and continuous sparsification (Louizos et al., 2018; Jang et al., 2017), we relax the discrete constraint by introducing continuous structural parameters, specifically the projection matrices \mathbf{W}_{read} . The temperature τ serves as a homotopy parameter: high values define a search space over the continuous probability simplex for

```

1 import numpy as np
2 def parity_last2(input_seq):
3     # V0_input
4     input_arr = np.array(input_seq, dtype
5                           =float)
6     seq_len = input_arr.shape[0]
7     V0 = input_arr[:, 0]
8     # V1_Attn_LOH0
9     V1 = np.zeros(seq_len)
10    # Fixed offset 1
11    V1[1:] = V0[:-1]
12    # V2_Attn_LOH1
13    V2 = np.zeros(seq_len)
14    # Fixed offset 1
15    V2[1:] = V0[:-1]
16    # V3_MLP_LOM0
17    V3 = ((V1 + -0.41) * ((V0 - 0.41) *
18                        3.57)) + -0.61
19    # Output Head
20    output = -0.56 * V3 + 0.17 * V0 +
21           0.10 * V2 + 0.07 * V1
22    return output
    
```

↓ *symbolic simplification*

Simplified Expression: $y_t = x_t + x_{t-1} - 2x_t x_{t-1}$

Figure 3. Algorithm extraction results for the `parity_last2` task. The extracted code reveals that the model utilizes specific attention heads (e.g., `Attn_LOH0`) to retrieve the previous token, and specific sub-MLPs (e.g., `MLP_LOM0`) to perform non-linear transformations. The bottom panel presents the symbolic simplification $y_t = x_t + x_{t-1} - 2x_t x_{t-1}$, which is the algebraic formulation of the parity logic.

exploration, while annealing $\tau \rightarrow 0$ smoothly deforms the distribution toward simplex vertices for exploitation.

To validate these dynamics, in addition to the MSE loss (serving as the soft training objective $\mathcal{L}_{\text{soft}}$), we monitor two metrics: Structural Agreement ($\mathcal{A}(e)$) and Discretization Discrepancy ($\Delta(e)$). Let $\{\mathbf{p}_r^{(e)}\}_{r=1}^R$ be the set of all row-wise probability distributions derived from $S(\mathbf{W}_{\text{read}}, \tau)$ at epoch e , E the total number of epochs, and $\mathcal{L}_{\text{hard}}(e)$ the hard loss computed via deterministic argmax sampling. We define $\mathcal{A}(e) = \frac{1}{R} \sum_{r=1}^R \mathbb{I}(\arg \max \mathbf{p}_r^{(e)} = \arg \max \mathbf{p}_r^{(E)})$. And we further define $\Delta(e) = \mathcal{L}_{\text{hard}}(e) - \mathcal{L}_{\text{soft}}(e)$. As shown in Figure 5, we observe a distinct phase transition: the significant decline in $\Delta(e)$ occurs slightly later than that of $\mathcal{L}_{\text{soft}}$, concurrently with $\mathcal{A}(e)$ approaching 1.0 as annealing proceeds. This lag suggests a two-stage process where the model first achieves *soft convergence*—learning functional mappings via relaxed representations—before undergoing *structural crystallization*, thereby ensuring a robust transition from exploration to exploitation.

```

1 import numpy as np
2 def relu(x):
3     return np.maximum(0, x)
4 def extrema_prev2(input_seq, mode):
5     # V0_input
6     input_arr = np.array(input_seq, dtype
7                             =float)
8     seq_len = input_arr.shape[0]
9     V0 = input_arr[:, 0]
10    # V1_Attn_LOH0
11    V1 = np.zeros(seq_len)
12    # Fixed offset 1
13    V1[1:] = V0[:-1]
14    # V3_MLP_LOM0, Output Head
15    if mode == "max": # maximum_prev2
16        V3 = ((V0 * -0.12) + relu(V1 *
17                                -1.00) + V0)) * -2.21) + ((V1 *
18                                -0.26) / 1.02)
19        output = 0.88 * V1 + -0.45 * V3 +
20                0.12 * V0
21    else: # minimum_prev2
22        V3 = 1.43 * (V0 + ((3.49 * relu(
23                                V1 - V0)) - V1) - (V1 * 1.04)))
24        output = 0.42 * V1 + 0.29 * V0 +
25                -0.20 * V3
26    return output

```

⇓ *symbolic simplification*

Simplified Expressions:

$$\begin{aligned} \max(x_t, x_{t-1}) &= x_{t-1} + \text{ReLU}(x_t - x_{t-1}) \\ \min(x_t, x_{t-1}) &= x_{t-1} - \text{ReLU}(x_{t-1} - x_t) \end{aligned}$$

Figure 4. Algorithm extraction results for `maximum_prev2` and `minimum_prev2` tasks. The top panel shows the raw code where sub-MLPs utilize ReLU functions to compare the current token x_t with the previous token x_{t-1} . The bottom panel presents the simplified expressions, verifying that the model correctly reconstructs the extrema functions using the ReLU-based algebraic identities.

6.2. Controllability via Inductive Biases

Unlike standard code LLMs, which synthesize programs based on opaque statistical patterns, our Discrete Transformer offers a unique advantage: interpretability-aware controllability. In scientific discovery, researchers often seek not just any solution, but a specific form of algorithm that aligns with domain knowledge (Schmidt & Lipson, 2009; Udrescu & Tegmark, 2020; Cranmer et al., 2020). We address this need by explicitly manipulating the architectural constraints and training configurations of our model to impose inductive biases, thereby steering the solution space.

We demonstrate this controllability through two intervention scenarios. First, we manipulate architectural primitives. In the `maximum_prev2` task, the unconstrained model typically solves maximization via MLP-based arithmetic approximation (exploiting ReLU non-linearity). To test if

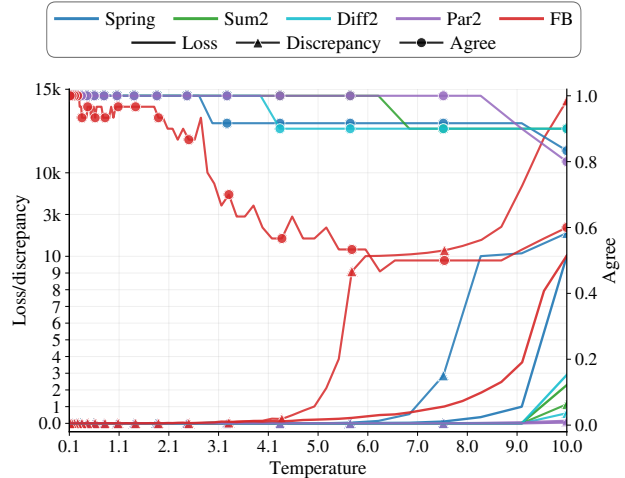


Figure 5. Training dynamics exhibit a clear phase transition: the loss decreases earlier, while the pronounced drop in Discrepancy occurs slightly later, coinciding with Agreement approaching 1.0 during temperature annealing from 10.0 to 0.1. The abbreviations Spring, Sum2, Diff2, Par2, and FB denote the spring, sum_last2, diff_last2, parity_last2, and freebody tasks, respectively.

the model can switch algorithmic paradigms, we explicitly set the number of sub-MLPs to zero, removing its capacity for complex arithmetic. Consequently, the model adapts by shifting its entire mechanism to the Numerical Attention module. It discovers a “windowed max” attention pattern, solving the task by directly copying the largest value from the context rather than computing it. Second, we intervene in the information flow. In the spring task, the model typically learns the standard recurrence $y_t = y_{t-1} - y_{t-2} + x_t$. By masking the immediate history (y_{t-1}, y_{t-2}), we guide the model to bypass the standard path and discover a mathematically equivalent high-order recurrence: $y_t = -y_{t-3} + x_t + x_{t-1}$. These findings highlight the Discrete Transformer as a robust tool for intervenable algorithm discovery, capable of uncovering multiple equivalent logical paths underlying the same data distribution.

7. Conclusion and Outlook

In this work, we introduce the Discrete Transformer, a novel architecture that enables program synthesis via algorithm extraction directly from Transformer models. By enforcing a disentangled numerical residual stream and employing a smooth discrete optimization curriculum, our model decouples information routing from arithmetic computation, facilitating the extraction of concise, human-readable algorithms. Our experiments show that this framework not only matches the performance of RNN-based approaches across a range of algorithmic tasks, but also provides fine-grained controllability. Despite these advantages, our interpretability-oriented

design inevitably entails trade-offs in complexity, expressivity, and capacity. Nevertheless, we view these constraints as a necessary step toward Transformer interpretability, and envision future work bridging the gap between algorithmic extractability and richer compositional expressivity.

Impact Statement

This paper advances the fields of mechanistic interpretability and algorithm extraction by enabling the discovery of verifiable, human-readable programs from the Discrete Transformer. There are many potential societal consequences of our work, none of which we feel must be specifically highlighted here.

References

- Bricken, T., Templeton, A., Batson, J., Chen, B., Jermyn, A., Conerly, T., Turner, N., Anil, C., Denison, C., Askell, A., Lasenby, R., Wu, Y., Kravec, S., Schiefer, N., Maxwell, T., Joseph, N., Hatfield-Dodds, Z., Tamkin, A., Nguyen, K., McLean, B., Burke, J. E., Hume, T., Carter, S., Henighan, T., and Olah, C. Towards Monosemanticity: Decomposing Language Models with dictionary learning. *Transformer Circuits Thread*, 2023. URL <https://transformer-circuits.pub/2023/monosemantic-features/index.html>.
- Church, A. Application of recursive arithmetic to the problem of circuit synthesis. *Journal of Symbolic Logic*, 28 (4), 1963.
- CodeGemma Team, Zhao, H., Hui, J., Howland, J., Nguyen, N., Zuo, S., Hu, A., Choquette-Choo, C. A., Shen, J., Kelley, J., Bansal, K., Vilnis, L., Wirth, M., Michel, P., Choy, P., Joshi, P., Kumar, R., Hashmi, S., Agrawal, S., Gong, Z., Fine, J., Warkentin, T., Hartman, A. J., Ni, B., Korevec, K., Schaefer, K., and Huffman, S. CodeGemma: Open code models based on Gemma, 2024. URL <https://arxiv.org/abs/2406.11409>.
- Cranmer, M. Interpretable machine learning for science with PySR and SymbolicRegression.jl, 2023. URL <https://arxiv.org/abs/2305.01582>.
- Cranmer, M., Sanchez-Gonzalez, A., Battaglia, P., Xu, R., Cranmer, K., Spergel, D., and Ho, S. Discovering symbolic models from deep learning with inductive biases, 2020. URL <https://arxiv.org/abs/2006.11287>.
- Cunningham, H., Ewart, A., Riggs, L., Huben, R., and Sharkey, L. Sparse Autoencoders find highly interpretable features in Language Models, 2023. URL <https://arxiv.org/abs/2309.08600>.
- Elhage, N., Hume, T., Olsson, C., Schiefer, N., Henighan, T., Kravec, S., Hatfield-Dodds, Z., Lasenby, R., Drain, D., Chen, C., Grosse, R., McCandlish, S., Kaplan, J., Amodei, D., Wattenberg, M., and Olah, C. Toy models of superposition, 2022. URL <https://arxiv.org/abs/2209.10652>.
- Friedman, D., Wettig, A., and Chen, D. Learning Transformer programs. In Oh, A., Naumann, T., Globerson, A., Saenko, K., Hardt, M., and Levine, S. (eds.), *Advances in Neural Information Processing Systems 36: Annual Conference on Neural Information Processing Systems 2023, NeurIPS 2023, New Orleans, LA, USA, December 10 - 16, 2023*, 2023. URL http://papers.nips.cc/paper_files/paper/2023/hash/995f693b73050f90977ed2828202645c-Abstract-Conference.html.
- Geva, M., Caciularu, A., Wang, K., and Goldberg, Y. Transformer feed-forward layers build predictions by promoting concepts in the vocabulary space. In Goldberg, Y., Kozareva, Z., and Zhang, Y. (eds.), *Proceedings of the 2022 Conference on Empirical Methods in Natural Language Processing*, pp. 30–45, Abu Dhabi, United Arab Emirates, December 2022. Association for Computational Linguistics. doi: 10.18653/v1/2022.emnlp-main.3. URL <https://aclanthology.org/2022.emnlp-main.3/>.
- Gorishniy, Y., Rubachev, I., and Babenko, A. On embeddings for numerical features in tabular deep learning. *Advances in Neural Information Processing Systems*, 35: 24991–25004, 2022.
- Graves, A., Wayne, G., and Danihelka, I. Neural Turing machines, 2014. URL <https://arxiv.org/abs/1410.5401>.
- Guo, D., Zhu, Q., Yang, D., Xie, Z., Dong, K., Zhang, W., Chen, G., Bi, X., Wu, Y., Li, Y. K., Luo, F., Xiong, Y., and Liang, W. DeepSeek-Coder: When the large language model meets programming – the rise of code intelligence, 2024. URL <https://arxiv.org/abs/2401.14196>.
- Jang, E., Gu, S., and Poole, B. Categorical reparameterization with Gumbel-Softmax, 2017. URL <https://arxiv.org/abs/1611.01144>.
- Lai-Dang, Q.-V., Kang, T., and Son, S. Adaptive Transformer programs: Bridging the gap between performance and interpretability in Transformers. In Yue, Y., Garg, A., Peng, N., Sha, F., and Yu, R. (eds.), *International Conference on Representation Learning*, volume 2025, pp. 62785–62807, 2025. URL https://proceedings.iclr.cc/paper_files/paper/2025/f

- [ile/9d5609613524ecf4f15af0f7b31abca4-Paper-Conference.pdf](https://arxiv.org/abs/1910.10683).
- Lindner, D., Kramár, J., Farquhar, S., Rahtz, M., McGrath, T., and Mikulik, V. Tracr: Compiled Transformers as a laboratory for interpretability. In Oh, A., Naumann, T., Globerson, A., Saenko, K., Hardt, M., and Levine, S. (eds.), *Advances in Neural Information Processing Systems 36: Annual Conference on Neural Information Processing Systems 2023, NeurIPS 2023, New Orleans, LA, USA, December 10 - 16, 2023*. URL http://papers.nips.cc/paper_files/paper/2023/hash/771155abaae744e08576f1f3b4b7ac0d-Abstract-Conference.html.
- Loshchilov, I. and Hutter, F. Decoupled weight decay regularization, 2019. URL <https://arxiv.org/abs/1711.05101>.
- Louizos, C., Welling, M., and Kingma, D. P. Learning sparse neural networks through l_0 regularization, 2018. URL <https://arxiv.org/abs/1712.01312>.
- Ma, H., Narayanaswamy, A., Riley, P., and Li, L. Evolving symbolic density functionals. *Science Advances*, 8(36): eabq0279, 2022.
- Martins, A. F. T. and Astudillo, R. F. From softmax to sparsemax: A sparse model of attention and multi-label classification, 2016. URL <https://arxiv.org/abs/1602.02068>.
- Meurer, A., Smith, C. P., Paprocki, M., Certík, O., Kirpichev, S. B., Rocklin, M., Kumar, A., Ivanov, S., Moore, J. K., Singh, S., Rathnayake, T., Vig, S., Granger, B. E., Muller, R. P., Bonazzi, F., Gupta, H., Vats, S., Johansson, F., Pedregosa, F., Curry, M. J., Terrel, A. R., Roucka, S., Saboo, A., Fernando, I., Kulal, S., Cimrman, R., and Scopatz, A. M. SymPy: symbolic computing in Python. *PeerJ Comput. Sci.*, 3:e103, 2017. doi: 10.7717/PEERJ-CS.103. URL <https://doi.org/10.7717/peerj-cs.103>.
- Michaud, E. J., Liao, I., Lad, V., Liu, Z., Mudide, A., Loughridge, C., Guo, Z. C., Kheirkhah, T. R., Vukelić, M., and Tegmark, M. Opening the AI black box: program synthesis via mechanistic interpretability, 2024. URL <https://arxiv.org/abs/2402.05110>.
- Paszke, A., Gross, S., Massa, F., Lerer, A., Bradbury, J., Chanan, G., Killeen, T., Lin, Z., Gimelshein, N., Antiga, L., Desmaison, A., Köpf, A., Yang, E., DeVito, Z., Raison, M., Tejani, A., Chilamkurthy, S., Steiner, B., Fang, L., Bai, J., and Chintala, S. PyTorch: An imperative style, high-performance deep learning library, 2019. URL <https://arxiv.org/abs/1912.01703>.
- Raffel, C., Shazeer, N., Roberts, A., Lee, K., Narang, S., Matena, M., Zhou, Y., Li, W., and Liu, P. J. Exploring the limits of transfer learning with a unified text-to-text Transformer, 2023. URL <https://arxiv.org/abs/1910.10683>.
- Rozière, B., Gehring, J., Gloeckle, F., Sootla, S., Gat, I., Tan, X. E., Adi, Y., Liu, J., Sauvestre, R., Remez, T., Rapin, J., Kozhevnikov, A., Evtimov, I., Bitton, J., Bhatt, M., Ferrer, C. C., Grattafiori, A., Xiong, W., Défossez, A., Copet, J., Azhar, F., Touvron, H., Martin, L., Usunier, N., Scialom, T., and Synnaeve, G. Code Llama: Open foundation models for code, 2024. URL <https://arxiv.org/abs/2308.12950>.
- Savarese, P., Silva, H., and Maire, M. Winning the lottery with continuous sparsification, 2021. URL <https://arxiv.org/abs/1912.04427>.
- Schmidt, M. and Lipson, H. Distilling free-form natural laws from experimental data. *Science*, 324(5923):81–85, 2009.
- Shojaee, P., Meidani, K., Gupta, S., Farimani, A. B., and Reddy, C. K. LLM-SR: Scientific equation discovery via programming with large language models, 2025. URL <https://arxiv.org/abs/2404.18400>.
- Udrescu, S.-M. and Tegmark, M. AI Feynman: A physics-inspired method for symbolic regression. *Science Advances*, 6(16):eaay2631, 2020.
- Udrescu, S.-M., Tan, A., Feng, J., Neto, O., Wu, T., and Tegmark, M. AI Feynman 2.0: Pareto-optimal symbolic regression exploiting graph modularity, 2020. URL <https://arxiv.org/abs/2006.10782>.
- Weiss, G., Goldberg, Y., and Yahav, E. Thinking like Transformers. In Meila, M. and Zhang, T. (eds.), *Proceedings of the 38th International Conference on Machine Learning*, volume 139 of *Proceedings of Machine Learning Research*, pp. 11080–11090. PMLR, 18–24 Jul 2021. URL <https://proceedings.mlr.press/v139/weiss21a.html>.
- Zhang, Y., Du, W., Jin, D., Fu, J., and Jin, Z. Finite state automata inside Transformers with Chain-of-Thought: A mechanistic study on state tracking, 2025. URL <https://arxiv.org/abs/2502.20129>.

A. Smooth Transition Mechanism for Discrete Optimization

To train the discrete selection parameters in our discretized reading and Numerical Attention modules, we address the non-differentiability of hard selection while avoiding the pitfalls of standard relaxation methods. While Gumbel-Softmax enables differentiable sampling, it often struggles to escape local optima and fails to promote the strict sparsity essential for interpretability. To address this, we incorporate a smooth transition mechanism (Lai-Dang et al., 2025), which dynamically interpolates between Gumbel-Softmax and Sparsemax (Martins & Astudillo, 2016) throughout the training process. The hybrid sampling vector $\mathbf{p} \in \mathbb{R}^{N_i}$ is defined as:

$$\mathbf{p} = (1 - \alpha(\tau))\mathbf{p}_{\text{soft}} + \alpha(\tau)\mathbf{p}_{\text{sparse}}, \quad (8)$$

where \mathbf{p}_{soft} and $\mathbf{p}_{\text{sparse}}$ denote sample vectors drawn from Gumbel-Softmax and Gumbel-Sparsemax distributions, respectively. The interpolation factor $\alpha(\tau)$ is a temperature-dependent function, defined as $\alpha(\tau) = \frac{\tau_1 - \tau}{\tau_1 - \tau_2}$ (where τ_1 denotes the initial temperature and τ_2 denotes the final temperature), which monotonically transitions from 0 to 1 as the temperature τ is geometrically annealed. This mechanism allows the model to prioritize exploration via Softmax in the early stages, before smoothly transitioning to Sparsemax to enforce sparsity and deterministic selection (exploitation) in later stages. Ultimately, this ensures convergence to concise, interpretable program structures.

B. Unmatched Heads

Our analysis reveals that the “unmatched heads” do not represent missing algorithmic primitives, but rather manifest as computational noise or redundancy. Specifically, we observe that these heads are generally rendered ineffective through two primary mechanisms: by being suppressed with negligible magnitudes, or by being ignored by higher-layer modules.

For instance, in the `bitwise_and` task, the head labeled `Attn_LOH1` exhibits a disordered attention matrix that matches neither location-based nor content-based patterns. However, symbolic tracing of the computational graph confirms that its output variable is an orphan variable: it is not selected as an input by any subsequent modules nor aggregated by the final output projection. Similarly, in the `minimum_prev2` task with the number of sub-MLPs constrained to zero, we observe that the head labeled `Attn_LOH1` behaves as an unmatched head. Since its output is disconnected from the valid execution path, this lack of interpretability does not impede successful extraction of the underlying algorithm.

C. Experiment Details

Datasets The investigated tasks probe specific capabilities of neural networks, such as arithmetic reasoning, variable tracking, and non-linear composition. We categorize them into three logical tiers based on their underlying complexity:

- **Linear Arithmetic.** This category involves linear transformations. *Non-state-tracking* tasks (e.g., `sum_last2`) require only local attention within a fixed window. In contrast, *State-tracking* tasks (e.g., `sum_last`) require the model to maintain a persistent memory state—implicitly simulating a finite state automaton (Zhang et al., 2025)—to compute the recurrent state over the sequence. Moreover, to evaluate generalization beyond pure arithmetic, we include tasks derived from classical mechanics (`freebody`, `gravity`, and `spring`), which are mathematically reducible to linear state-tracking tasks.
- **Non-Linear Composition.** These tasks necessitate non-linear activation logic. Variants range from local operations like `parity_last2` and `maximum_prev2` to global state-tracking tasks like `add_mod_3`. Success here requires the Numerical MLP to approximate non-linear functions (e.g., XOR) rather than simple linear aggregation.
- **Continuous Dynamics.** While the preceding two categories primarily focus on discrete variables, this category encompasses mathematical and physical tasks that require modeling and processing continuous-valued variables, such as `exponential_moving_average` and `free_fall_height`.

Training Details All models adopt a decoder-only architecture implemented in PyTorch (Paszke et al., 2019), optimized via AdamW (Loshchilov & Hutter, 2019) to minimize MSE. The training dataset consists of 1,000,000 samples. Unless otherwise specified, both the input and output sequences have a fixed length of 10. We employ a cosine annealing schedule to decay the learning rate from 0.05 to 1×10^{-6} over 50 epochs with a batch size of 512. (For the `freebody` and `gravity` tasks, models are trained for 100 epochs with an initial learning rate of 0.01.) To handle discrete optimization, we apply a

geometric annealing schedule to the sampling temperature τ , decreasing it from 10.0 to 0.1 to facilitate a gradual transition from continuous exploration to discrete selection. For each task, we conduct a grid search over the number of layers $\{1, 2\}$, attention heads $\{2, 3\}$, and sub-MLPs per layer $\{2, 3\}$. We run all experiments across three random seeds, reporting the mean performance and selecting the checkpoint with the best validation performance for subsequent analysis.

Task Formulation To facilitate algorithm extraction across varying positions, we design our task formulations to encourage the learning of position-invariant functions. Specifically, we categorize tasks according to their reliance on state-tracking: (1) Non-state-tracking tasks are formulated as Token-Tagging problems, requiring independent, element-wise predictions for each position. (2) State-tracking tasks are framed as Language Modeling problems, where the model performs autoregressive next-token prediction based on the input and historical context. To facilitate symbolic regression and align with the regression-oriented nature of these tasks, we adopt MSE as the training loss.

Symbolic Regression Details We apply PySR (Cranmer, 2023), a genetic-algorithm-based symbolic regression method, to identify the symbolic expression \hat{f} that minimizes the prediction error on \mathcal{D} . Specifically, we use PySR with its default hyperparameter settings; moreover, for nonlinear tasks, we introduce additional operators such as ReLU. And to ensure reproducibility, we set the random seed to 42. The overall runtime for extracting an algorithm from a model ranges from a few minutes to several tens of minutes.

D. Robustness of the Discrete Transformer

To evaluate the robustness of our framework under architectural variations, we investigate the impact of hyperparameters—specifically the number of layers, attention heads per layer, and sub-MLPs per layer—on both the convergence quality, measured by the MSE loss, and the complexity, quantified by the line count of the extracted program. We conduct experiments on the `sum_last2`, `parity_last2`, and `spring` tasks, varying the number of layers in $\{1, 2, 3, 4\}$, attention heads per layer in $\{0, 1, 2, 4, 8\}$, and sub-MLPs per layer in $\{0, 1, 2, 4, 8\}$.

Our results exhibit a clear threshold effect in expressive capacity. Once the architecture satisfies the minimal functional requirements of the target task (e.g., `sum_last2` requires at least one attention head to retrieve the token x_{t-1}), the Discrete Transformer reliably converges to a near-zero MSE loss (see Figure 6). Furthermore, we find that over-parameterization substantially alters the dynamics of the discrete search. Specifically, excessive capacity tends to inflate the length of the extracted programs due to structural redundancy: multiple modules may learn functionally equivalent behaviors (e.g., several attention heads learning the same retrieval pattern for x_{t-1}). The presence of redundant modules expands the search space and introduces noise during the exploration phase. Although this complicates optimization and may impair stability, we find that the issue can be effectively mitigated by adopting a slower temperature annealing schedule, which allows sufficient time for redundant components to resolve competition and converge to a valid discrete solution. Overall, these findings highlight the robustness of the Discrete Transformer to architectural hyperparameter variations.

E. Additional Synthesized Programs

In this section, we provide additional synthesized programs.

Table 2. Performance and parameters of the Discrete Transformer on the algorithmic benchmark. The columns Layers, Heads, and sub-MLPs correspond to the number of layers, the number of attention heads per layer, and the number of sub-MLPs per layer, respectively. Loss values are averaged MSE over three random seeds.

Task Name	Description	Layers	Heads	sub-MLPs	Train Loss
<i>Linear Arithmetic</i>					
sum_last2	Sum of the last two numbers	1	2	2	8.82×10^{-9}
diff_last2	Difference of the last two numbers	1	2	2	6.59×10^{-16}
sum	Cumulative sum of the sequence	1	2	2	1.71×10^{-14}
div_3	Binary division by 3	1	2	2	2.20×10^{-1}
freebody	Simulate freebody dynamics	2	2	3	9.57×10^{-11}
gravity	Simulate gravity dynamics	2	2	3	2.34×10^{-11}
spring	Simulate spring dynamics	1	2	2	1.41×10^{-7}
magnetic	Simulate magnetic dynamics	2	2	3	1.12×10^2
<i>Non-Linear Composition</i>					
parity_last2	Parity of the last two numbers	1	2	2	4.87×10^{-13}
maximum_prev2	Maximum of the last two numbers	1	2	2	1.11×10^{-6}
minimum_prev2	Minimum of the last two numbers	1	2	2	1.64×10^{-5}
unique_prev2	1 if last two numbers are equal	1	2	2	4.19×10^{-14}
bitwise_and	Bitwise AND	1	2	2	1.10×10^{-18}
bitwise_or	Bitwise OR	1	2	2	5.66×10^{-4}
bitwise_not	Bitwise NOT	1	2	2	1.44×10^{-17}
bitwise_xor	Bitwise XOR	1	2	2	6.74×10^{-20}
abs	Abs value of the number	1	2	2	2.69×10^{-14}
abs_of_diff	Abs difference of last two numbers	1	2	2	9.72×10^{-9}
parity	Cumulative parity	1	2	2	8.15×10^{-17}
parity_zeros	Cumulative parity of number of zeros	1	2	2	2.25×10^{-8}
add_mod_3	Cumulative sum modulo 3	1	2	2	9.72×10^{-13}
bit_dot_prod_mod_2	Cumulative dot product of bits mod 2	1	2	2	5.55×10^{-4}
bit_addition	Binary addition	2	4	4	2.49×10^{-2}
balanced_parenthesis	1 if parentheses are balanced	1	2	2	2.08×10^{-2}
<i>Continuous Dynamics</i>					
exponential_moving_average	Exponential moving average	1	2	2	1.62×10^{-13}
free_fall_height	Free-fall height	1	1	1	8.53×10^{-5}

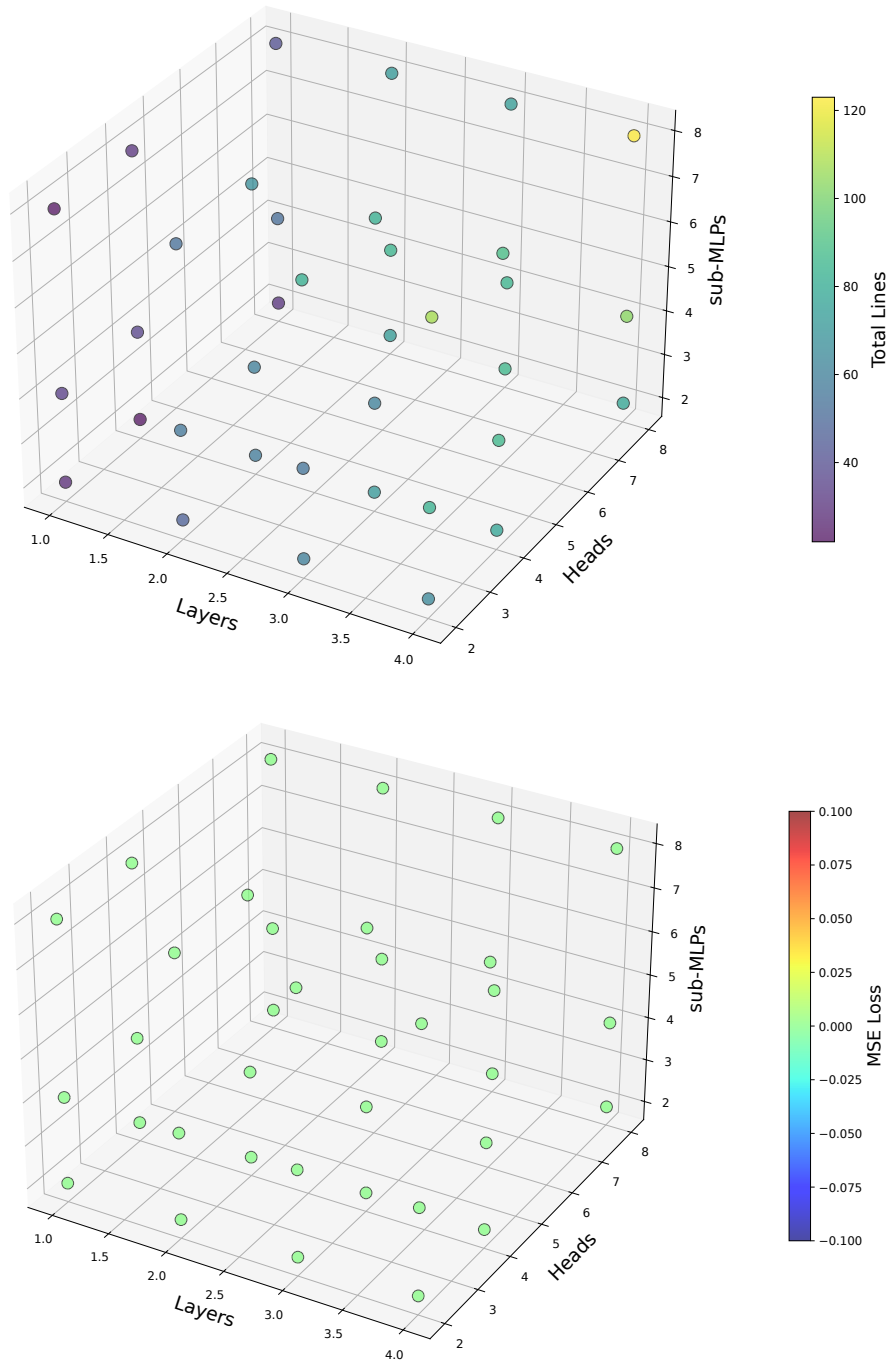


Figure 6. Robustness landscape: program complexity (Top) and convergence loss (Bottom) on the `sum_last2` task. Excessive model capacity often increases the length of the extracted programs due to redundancy, while exerting only a minor effect on the MSE loss.

```

1 import numpy as np
2 def maximum_prev2(input_seq):
3     # V0_input
4     input_arr = np.array(input_seq, dtype
5                             =float)
6     seq_len = input_arr.shape[0]
7     V0 = input_arr[:, 0]
8     # V1_Attn_LOH0
9     V1 = np.zeros(seq_len)
10    # windowed max
11    for t in range(seq_len):
12        V1[t] = np.max(V0[max(0, t-1): t
13                        +1])
14    # V2_Attn_LOH1
15    V2 = np.zeros(seq_len)
16    # windowed max
17    for t in range(seq_len):
18        V2[t] = np.max(V0[max(0, t-1): t
19                        +1])
20    # Output Head
21    output = 1.07 * V1 + -0.07 * V2
22    return output

```

```

1 import numpy as np
2 def minimum_prev2(input_seq):
3     # V0_input
4     input_arr = np.array(input_seq, dtype
5                             =float)
6     seq_len = input_arr.shape[0]
7     V0 = input_arr[:, 0]
8     # V1_Attn_LOH0
9     V1 = np.zeros(seq_len)
10    # windowed min
11    for t in range(seq_len):
12        V1[t] = np.min(V0[max(0, t-1): t
13                        +1])
14    # Output Head
15    output = 1.00 * V1
16    return output

```

```

1 import numpy as np
2 def spring(input_seq):
3     # V0_input
4     input_arr = np.array(input_seq, dtype
5                             =float)
6     seq_len = input_arr.shape[0]
7     V0 = input_arr[:, 0]
8     # V1_Attn_LOH0
9     V1 = np.zeros(seq_len)
10    # Fixed offset 9
11    V1[9:] = V0[:-9]
12    # V2_Attn_LOH1
13    V2 = np.zeros(seq_len)
14    # Fixed offset 10
15    V2[10:] = V0[:-10]
16    # V3_MLP_LOM0
17    V3 = np.full(seq_len, 0.02)
18    # V4_MLP_LOM1
19    V4 = np.full(seq_len, -0.11)
20    # V5_Attn_L1H0
21    V5 = np.zeros(seq_len)
22    # Fixed offset 2
23    V5[2:] = V0[:-2]
24    # V6_Attn_L1H1
25    V6 = np.zeros(seq_len)
26    # Fixed offset 2
27    V6[2:] = V4[:-2]
28    # V7_MLP_L1M0
29    V7 = np.full(seq_len, -0.03)
30    # Output Head
31    output = 1.00 * V1 + 1.00 * V2 +
32            -1.00 * V5 + 0.03 * V7 + -0.01 * V6
33    return output

```

Figure 7. Intervened synthesized programs revealing alternative logical pathways. Left: When MLP-based arithmetic is prohibited, the model solves `maximum_prev2` and `minimum_prev2` by shifting to a pure attention mechanism. The extracted code shows explicit *Windowed Extrema* attention patterns. Right: For the `spring` task, intervention in the information flow (masking recent history) forces the model to learn a high-order recurrence relation, validating the model’s ability to uncover multiple equivalent algorithms for the same data distribution.

```

1 import numpy as np
2 def sum_last(input_seq):
3     # V0_input
4     input_arr = np.array(input_seq, dtype
5                           =float)
6     seq_len = input_arr.shape[0]
7     V0 = input_arr[:, 0]
8     # V1_Attn_LOH0
9     V1 = np.zeros(seq_len)
10    # Fixed offset 9
11    V1[9:] = V0[:-9]
12    # Output Head
13    output = 1.00 * V0 + 1.00 * V1
14    return output

```

```

1 import numpy as np
2 def bitwise_and(input_seq):
3     # V0_input, V1_input
4     input_arr = np.array(input_seq, dtype
5                           =float)
6     seq_len = input_arr.shape[0]
7     V0 = input_arr[:, 0]
8     V1 = input_arr[:, 1]
9     # V4_MLP_L0M0
10    V4 = np.full(seq_len, 0.02)
11    # V5_MLP_L0M1
12    V5 = (((V0 - 0.49) * 3.28) / (V1 +
13    -0.52)) - 3.06) * 0.19
14    # Output Head
15    output = 0.49 * V1 + 0.48 * V0 + 0.40
16    * V5 + 0.02 * V4
17    return output

```

```

1 import numpy as np
2 def add_mod_3(input_seq):
3     # V0_input
4     input_arr = np.array(input_seq, dtype
5                           =float)
6     seq_len = input_arr.shape[0]
7     V0 = input_arr[:, 0]
8     # V1_Attn_LOH0
9     V1 = np.zeros(seq_len)
10    # Fixed offset 9
11    V1[9:] = V0[:-9]
12    # V2_Attn_LOH1
13    V2 = np.zeros(seq_len)
14    # Fixed offset 9
15    V2[9:] = V0[:-9]
16    # V3_MLP_L0M0
17    V3 = ((-0.70 / ((V0 + V1) + 0.59) *
18    -0.56)) - 1.69) + (1.05 / (V0 + (V1 -
19    2.53)))
20    # Output Head
21    output = -0.53 * V3 + 0.47 * V2 +
22    -0.32 * V1 + 0.16 * V0
23    return output

```

Figure 8. Synthesized programs for sum_last (Top Left), bitwise_and (Bottom Left), and add_mod_3 (Right).

```

1 import numpy as np
2 def freebody(input_seq):
3     # V0_input
4     input_arr = np.array(input_seq, dtype
5                           =float)
6     seq_len = input_arr.shape[0]
7     V0 = input_arr[:, 0]
8     # V1_Attn_LOH0
9     V1 = np.zeros(seq_len)
10    # Fixed offset 9
11    V1[9:] = V0[:-9]
12    # V2_Attn_LOH1
13    V2 = np.zeros(seq_len)
14    # Fixed offset 10
15    V2[10:] = V0[:-10]
16    # V4_MLP_LOM1
17    V4 = -0.26*V0 + 0.04
18    # V5_MLP_LOM2
19    V5 = -0.21*V0 + -0.04
20    # V6_Attn_L1H0
21    V6 = np.zeros(seq_len)
22    # Fixed offset 2
23    V6[2:] = V4[:-2]
24    # V7_Attn_L1H1
25    V7 = np.zeros(seq_len)
26    # Fixed offset 2
27    V7[2:] = V5[:-2]
28    # Output Head
29    output = 1.19 * V0 + 1.06 * V7 + 1.06
30            * V6 + 1.00 * V1 + -0.65 * V4 +
31            -0.65 * V5 + 0.50 * V2
32    return output

```

```

1 import numpy as np
2 def gravity(input_seq):
3     # V0_input
4     input_arr = np.array(input_seq, dtype
5                           =float)
6     seq_len = input_arr.shape[0]
7     V0 = input_arr[:, 0]
8     # V1_Attn_LOH0
9     V1 = np.zeros(seq_len)
10    # Fixed offset 9
11    V1[9:] = V0[:-9]
12    # V2_Attn_LOH1
13    V2 = np.zeros(seq_len)
14    # Fixed offset 10
15    V2[10:] = V0[:-10]
16    # V4_MLP_LOM1
17    V4 = 0.00
18    # V5_MLP_LOM2
19    V5 = -0.40*V0 + -3.05
20    # V6_Attn_L1H0
21    V6 = np.zeros(seq_len)
22    # Fixed offset 2
23    V6[2:] = V5[:-2]
24    # V7_Attn_L1H1
25    V7 = np.zeros(seq_len)
26    # Fixed offset 2
27    V7[2:] = V4[:-2]
28    # Output Head
29    output = 1.24 * V6 + 1.20 * V0 + 1.00
30            * V1 + -0.74 * V5 + 0.50 * V2 +
31            -0.01 * V4 + 0.01 * V7
32    return output

```

```

1 import numpy as np
2 def spring(input_seq):
3     # V0_input
4     input_arr = np.array(input_seq, dtype
5                           =float)
6     seq_len = input_arr.shape[0]
7     V0 = input_arr[:, 0]
8     # V1_Attn_LOH0
9     V1 = np.zeros(seq_len)
10    # Fixed offset 9
11    V1[9:] = V0[:-9]
12    # V2_Attn_LOH1
13    V2 = np.zeros(seq_len)
14    # Fixed offset 1
15    V2[1:] = V0[:-1]
16    # V4_MLP_LOM1
17    V4 = (V2 + ((V1 - ((V1 + 2.26) + (V2
18    - 1.54))) * 2.00)) + (V2 + 1.43)
19    # Output Head
20    output = -1.00 * V2 + 1.00 * V0 +
21            1.00 * V1 + 0.04 * V4
22    return output

```

Figure 9. Synthesized programs for freebody (Top Left), spring (Bottom Left), and gravity (Right).